ZnO Spintronics and Nanowire Devices

S.J. PEARTON,[1,4] D.P. NORTON,[1] Y.W. HEO,[1] L.C. TIEN,[1] M.P. IVILL,[1] Y. LI,[1] B.S. KANG,[2] F. REN,[2] J. KELLY,[3] and A.F. HEBARD[3]

1.—Materials Science Engineering, University of Florida, Gainesville, FL 32611. 2.—Chemical Engineering, University of Florida. 3.—Physics, University of Florida. 4.—E-mail: spear@mse.ufl.edu

ZnO is a very promising material for spintronics applications, with many groups reporting room-temperature ferromagnetism in films doped with transition metals during growth or by ion implantation. In films doped with Mn during pulsed laser deposition (PLD), we find an inverse correlation between magnetization and electron density as controlled by Sn-doping. The saturation magnetization and coercivity of the implanted single-phase films were both strong functions of the initial anneal temperature, suggesting that carrier concentration alone cannot account for the magnetic properties of ZnO:Mn and factors such as crystalline quality and residual defects play a role. Plausible mechanisms for ferromagnetism include the bound magnetic polaron model or exchange that is mediated by carriers in a spin-split impurity band derived from extended donor orbitals. The progress in ZnO nanowires is also reviewed. The large surface area of nanorods makes them attractive for gas and chemical sensing, and the ability to control their nucleation sites makes them candidates for microlasers or memory arrays. Single ZnO nanowire depletion-mode metal-oxide semiconductor field effect transistors exhibit good saturation behavior, threshold voltage of ~−3 V, and a maximum transconductance of 0.3 mS/mm. Under ultraviolet (UV) illumination, the drain-source current increased by approximately a factor of 5 and the maximum transconductance was ~5 mS/mm. The channel mobility is estimated to be ~3 $cm^2/V\dot{s}s$, comparable to that for thin film ZnO enhancement mode metal-oxide semiconductor field effect transistors (MOSFETs), and the on/off ratio was ~25 in the dark and ~125 under UV illumination. The Pt Schottky diodes exhibit excellent ideality factors of 1.1 at 25°C, very low reverse currents, and a strong photoresponse, with only a minor component with long decay times thought to originate from surface states. In the temperature range from 25°C to 150°C, the resistivity of nanorods treated in H_2 at 400°C prior to measurement showed an activation energy of 0.089 eV and was insensitive to the ambient used. By contrast, the conductivity of nanorods not treated in H_2 was sensitive to trace concentrations of gases in the measurement ambient even at room temperature, demonstrating their potential as gas sensors. Sensitive pH sensors using single ZnO nanowires have also been fabricated.

Key words: ZnO, nanorods, ferromagnetism

INTRODUCTION

The use of carrier spin, in addition to charge, appears promising for a new class of devices such as polarized light emitters, chips that integrate memory and microprocessor functions, magnetic devices exhibiting gain, and ultra-low power transistors.[1–10] The use of carrier spin in metallic multilayers forms the basis for hard drives in information storage. The control of spin-dependent phenomena in electronic oxides or more conventional semiconductors may lead to devices such as spin–light-emitting diodes (spin-LEDs), spin–field effect transistors (spin-FETs), and spin qubits for quantum computers.[1,2,8] A key requirement in realizing most devices based on spins in solids is that the host material be ferromagnetic above room temperature. In addition, it is necessary to have both efficient

(Received May 10, 2005; accepted August 25, 2005)

spin-polarized carrier injection and transport. It is generally believed that it is necessary to achieve single-phase dilute magnetic oxides in order to realize useful devices, since it is the polarized carrier population that carries the spin information, although there may be applications for multiphase materials in magneto-optical applications. The usefulness of ferromagnetic wide bandgap semiconductors for spintronic applications requires the existence of a coupling between ferromagnetic and semiconducting properties, independent of the actual microstructure of the system under study. If precipitates or clusters below detectable size limits are present and responsible for the ferromagnetism and if the carriers do not mediate the ferromagnetic interaction, then the usefulness of such materials in spintronics should be called into question. On the other hand, it is not clear that the presence of ferromagnetic nanoclusters excludes a carrier-mediated interaction. Isolated by themselves, such clusters should act as superparamagnets.

FERROMAGNETISM IN ZnO

Of the semiconducting oxides, ZnO offers significant potential in providing charge, photonic, and spin-based functionality.[11–36] ZnO is a direct, wide bandgap semiconductor with potential utility in UV photonics and transparent electronics. For spintronics, theoretical predictions suggest that room-temperature carrier-mediated ferromagnetism should be possible in ZnO, albeit for p-type material. Unfortunately, the realization of p-type ZnO has proven difficult until recently. Ab initio calculations do predict ferromagnetism in n-type ZnO-doped with most transition metal ions, including Co and Cr, but predict no ferromagnetism for Mn-doped ZnO.[30] This is consistent with experimental results in which ferromagnetism is not observed in Mn-doped ZnO that is n type due to group III impurities (Table I). However, ferromagnetism has been observed in n-type Mn-implanted and Sn-doped ZnO crystals. Sn (a group IV element) serves as a doubly ionized donor impurity. The specific role of Sn dopant in enabling ferromagnetism in Mn-doped ZnO is unclear. The Sn may simply provide carriers, albeit electrons, that effectively mediate the spin interactions. The Sn dopant might alternatively form complexes with Mn, resulting in both Mn^{+2} and Mn^{+3} sites that could yield a ferromagnetic ordering.

Several groups have investigated the magnetic properties of TM-doped ZnO, as summarized in Table II. In all of these studies, the ZnO material was n type. The magnetic properties of Ni-doped ZnO thin films were reported by a number of groups.[9,23,25] For films doped with 3–25at.%Ni, ferromagnetism was observed at 2 K. Above 30 K, superparamagnetic behavior was observed. Fukumura et al.[9] have shown that epitaxial thin films of Mn-doped ZnO can be obtained by pulsed-laser deposition, with Mn substitution as high as 35%, while maintaining the wurtzite structure. This is well above the equilibrium solubility limit of ~13% and illustrates the utility of low-temperature epitaxial growth in achieving metastable solubility in thin films. Co-doping with Al resulted in n-type material with carrier concentration in excess of 10^{19} cm^{-3}. Large magnetoresistance was observed in the films, but no evidence for ferromagnetism was reported. However, Jung et al.[20] recently reported ferromagnetism in Mn-doped ZnO epitaxial films, with a Curie temperature of 45 K. The discrepancy appears to lie in differing film-growth conditions.

Ion implantation can be used to survey the magnetic properties of a number of transition metal dopants in various semiconducting oxide materials. High-temperature ferromagnetism was observed in ZnO crystals implanted with transition metal dopants, including Co and Mn, Co-doped with Sn.[4,5,21,22] In the case of Mn Co-doped with Sn, the Sn ions are provided as doubly ionized donors. This result differs from that reported for Mn-doped ZnO-doped n-type with Al or Ga, and suggests that group IV dopants may behave differently than shallow group III donors in terms of interaction with magnetic dopants. If carrier-mediated mechanisms are responsible, one must explain why the behavior depends on the specific cation dopant species chosen (Sn versus Al, Ga). Insight into this issue may reside in the fact that doping via a multi-ionized impurity likely introduces relatively deep donor levels in the energy gap. Conduction from deep donors is often due to the impurity band or hopping conduction, as opposed to conventional free electrons excited to the conduction band. Any carrier-mediated processes would be dependent on the relevant conduction mechanisms. This result appears to contradict the expectation that, in the absence of a shallow acceptor level, the dominant exchange mechanism is short-range superexchange, which,

Table I. Oxidation and Charge States Expected for Some Candidate Transition Metals in ZnO[9]

ZnO	$3d^3$	$3d^4$	$3d^5$	$3d^6$
Acceptor (negative charge)	—	—	Cr^{+}	Mn^{+}
Neutral	—	Cr^{2+}	Mn^{2+}	Fe^{2+}
Donor (positive charge)	Cr^{3+}	Mn^{3+}	Fe^{3+}	—
Double donor (2^{+} charge)	Mn^{4+}	Fe^{4+}	—	—
p-ZnO Cr	Cr^{3+} (donor)	—	—	—
p-ZnO Mn	—	—	Mn^{2+} (neutral acceptor)	—
p-ZnO Fe	—	—	Fe^{3+} (donor)	—

Table II. Potential Second Phases That Can Form in Mn-and Co-Doped ZnO and Their Magnetic Properties

Phase	Nature of Magnetism	Applicable Magnetic Temperature (K)
Mn	Antiferromagnetic	100
Co	Ferromagnetic	1373
MnO	Antiferromagnetic	122
MnO_2	Antiferromagnetic	84
	Antiferromagnetic	17
	Weak ferromagnetic	44
Mn_3O_4	Ferromagnetic	1443
	Ferromagnetic	42
	Ferrimagnetic	46
$ZnMn_2O_4$	Ferromagnetic	1298
$Zn_{0.9}Mn_{0.1}O$	Ferromagnetic	30
$Zn_{0.7}Mn_{0.3}O$	Ferromagnetic	45
MnSi	Ferromagnetic	29.5
MnZn (15% Mn)	Ferromagnetic	150
$MnAu_4$	Ferromagnetic	360
$MnAu_2$	Ferromagnetic	365
CoO	Antiferromagnetic	291
$Zn_{0.95}Co_{0.5}O$	Ferromagnetic	280
$Zn_{0.85}Co_{0.15}O$	Ferromagnetic	300
$Zn_{0.75}Co_{0.15}O$	Ferromagnetic	280
CoZn	Ferromagnetic	468

for Mn^{+2} in ZnO, should favor antiferromagnetic ordering. The results will be discussed in detail in a later section. Despite the uncertainty in the mechanism, these results (high-temperature ferromagnetism in Co and Mn, Sn-doped ZnO) indicate a pathway for exploring spintronics in ZnO materials.

The ionic radius of Mn^{+2} (0.66 Å) is relatively close to that for Zn (0.60 Å), suggesting moderate solid solubility without phase segregation. As such, the primary transition metal dopant of interest will be Mn. Chromium and cobalt presents the possibility of achieving ferromagnetism in ZnO via doping with magnetic ions for which the net superexchange coupling is ferromagnetic. Low-temperature ferromagnetic behavior has been observed in Cr-based spinel semiconductors. Theoretical results predict that Cr-doping in II-VI semiconductors should result in ferromagnetism.[7,12]

Figure 1 shows the magnetization versus field behavior at 300 K for Sn-doped ZnO samples implanted with 3at.%Mn and 5at.%Mn. Hysteretic behavior is clearly observed, consistent with ferromagnetism. At 10 K, the coercive field in the 3at.%Mn-doped sample is 250 Oe. It must be noted that other possible explanations for hysteretic M versus H behavior that are remotely possible include superparamagnetism and spin-glass effects. Magnetization measurements were also performed on Sn:ZnO crystals that were not subjected to the Mn implant. This was done to eliminate the possibility that spurious transition metal impurities might be responsible for the magnetic response. The Sn-doped ZnO crystals exhibit no magnetic hysteresis, showing that Mn-doping is responsible for the behavior. To track the hysteretic behavior in the implanted samples as a function of temperature, both field-cooled and zero-field-cooled

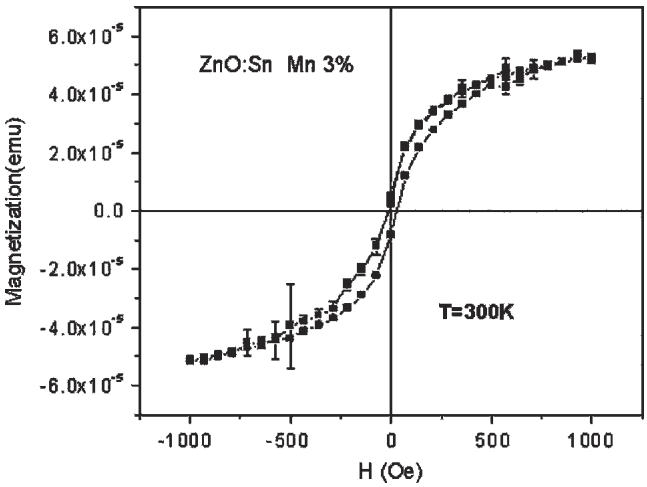

Fig. 1. Hysteresis loops in Sn-doped ZnO implanted with Mn.

magnetization measurements were performed from 4.2 K to 300 K. By taking the difference between these two quantities, the para and diamagnetic contributions to the magnetization can be subtracted, leaving only a measure of the hysteretic ferromagnetic regime. For the 3at.%Mn sample, in particular, a robust ferromagnetic signature is observed to persist up to temperatures >300 K.

While assigning the origin of ferromagnetism in transition-metal-doped semiconductors, one must carefully consider the possibility that secondary phase formation is responsible. First, metallic Mn is antiferromagnetic, with a Nèel temperature of 100 K. In addition, nearly all of the possible Mn-based binary and ternary oxide candidates are antiferromagnetic. The exception to this is Mn_3O_4, which is ferromagnetic with a Curie temperature

of 46 K in thin films. Table II shows a compilation of reported magnetic behavior characteristics of potential second phases that could form in either Mn or Co-doped ZnO. X-ray diffraction (XRD) measurements on the implanted samples showed no evidence for Mn-O phases, although it is recognized that diffraction is limited in detecting secondary phases that may represent a fraction of a percent of total volume in the implanted region. However, even if this phase were present, it could not account for the remarkably high ferromagnetic transition temperature of ~300 K observed for the Mn-implanted ZnO:Sn crystals. It must also be noted that the Mn concentrations used in this study were well below the solid solubility limit of Mn in ZnO. Increasing the Mn content from 3at.% to 5at.% resulted in a significant decrease in the relative magnetization response. This provides strong evidence, albeit indirect, that the magnetization is not due to any precipitating secondary phase. If the formation of a secondary Mn-related phase were responsible for the ferromagnetic behavior, an increase in Mn concentration would presumably increase the secondary phase volume fraction and related magnetization signature. Instead, the opposite behavior is observed.

One can postulate as to the mechanism by which Sn-doping yields ferromagnetic interactions among the Mn ions. First, the Sn ions may simply provide carriers or bound donor states with extended wavefunctions that mediate interactions among the Mn ions. The Sn dopants may alternatively form complexes with the Mn ions, yielding a distribution of Mn^{+3} sites. In this case, the mixture of Mn^{+2}/Mn^{+3} sites could yield ferrimagnetic ordering through superexchange interaction. With this, the magnetic moment/Mn ion should increase with Sn-doping even if the measured conductivity changes very little. It should be noted that very little is known about the behavior of Sn in ZnO. Identifying the location of the energy state associated with Sn in ZnO would be most useful in the interpretation of magnetic properties when Co-doped with Mn. One could also look for shifts in the Sn or Mn dopant state location as the other dopant is added.

The observation that a doubly ionized donor (Sn) leads to ferromagnetic interactions among Mn atoms in ZnO raises the question as to whether deep states are, in general, effective in mediating ferromagnetism. Of particular interest are the theoretical predictions that ferromagnetism above room temperature should be possible in Mn-doped ZnO that is p type. Given the difficulty in realizing a shallow acceptor in ZnO, an obvious experiment, using the results for the Mn Co-doped with a deep donor (Sn), is to Co-dope Mn with a deep acceptor. Attractive deep acceptors for addressing this question are Cu and As. Copper-doping introduces an acceptor level with an energy ~0.17 eV below the conduction band. There is a large ionic radii mismatch for As (2.22 Å) on the O (1.38 Å) site, suggesting limited solid solubility for these anions. Nevertheless, p-n junctionlike behavior has been reported between an n-type ZnO film on GaAs subjected to annealing. In this case, a p-type layer was reportedly produced at the GaAs/ZnO interface. Further understanding of group V substitution in ZnO requires the study of doped materials that are free from complications of reactive substrates or interfacial layers. The primary interest is to investigate whether the deep acceptor states from Cu or As mediate ferromagnetic interactions in TM-doped ZnO.

For practical application in spintronic devices, the Curie temperature should be well above room temperature. As discussed earlier, theory suggests that the Curie temperature will tend to increase with decreasing cation mass. In addition, there is phenomenological evidence that T_c increases with increasing gap. Fortuitously, for Mn-doped ZnO:Sn, the only ferromagnetic secondary phase candidate is the Mn_3O_4 spinel. None of the other possible secondary phases involving combinations of Zn, Mn, O, and Sn yield a known ferromagnetic material. The high-temperature ferromagnetism in Mn-implanted ZnO:Sn crystals cannot be attributed to Mn_3O_4 as the T_c is much higher in the Mn-doped ZnO than for the Mn_3O_4 phase.

In addition to transmission electron microscopy (TEM), one can also use XRD to search for secondary phases within the films. Despite the obvious sensitivity limitations involved in detecting impurity phases that represent only 1–5 vol.% of a thin-film sample, we have been able to detect nanoscale precipitates in transition metal implanted samples. This is demonstrated for Co-implanted ZnO. Epitaxial $(Zn_{1-x}Co_x)O$ (x = 0.05–0.25) exhibits high-temperature ferromagnetism with T_c greater than 300 K. The ferromagnetic behavior is assigned to substitutional Co on the Zn site. Monte Carlo simulations of the indirect exchange interaction of Co-doped ZnO also predict ferromagnetism in these materials. SQUID magnetometry measurements of Co-doped ZnO clearly indicate ferromagnetism, as is shown in Fig 2. However, a careful examination of the XRD θ-2θ scan along the surface normal, shown in Fig. 2b, indicates the presence of Co precipitates. A Co (110) peak is clearly evident. From the width of the peak, the size of the cobalt precipitates can be estimated to be approximately 3.6 nm. Table III Summarizes results for magnetism in ZnO.

It should be noted that the presence of magnetic precipitates may mask an underlying carrier-mediated ferromagnetism due to substitutional doping. In this case, a more direct means of measuring the spin properties of the semiconductor carrier population is needed. Much of the research activity being presently pursued in spintronics is directed at demonstrating device structures (spin-LED, spin-FET) that differentiate spin polarization distribution among the electron/hole population in the semiconductor.

ZnO Nanowire Devices

We have fabricated many types of ZnO nanowire devices, including MOSFETs, diodes, and UV sensors. In this work, we will only discuss more recent work on pH sensors. There is emerging interest in

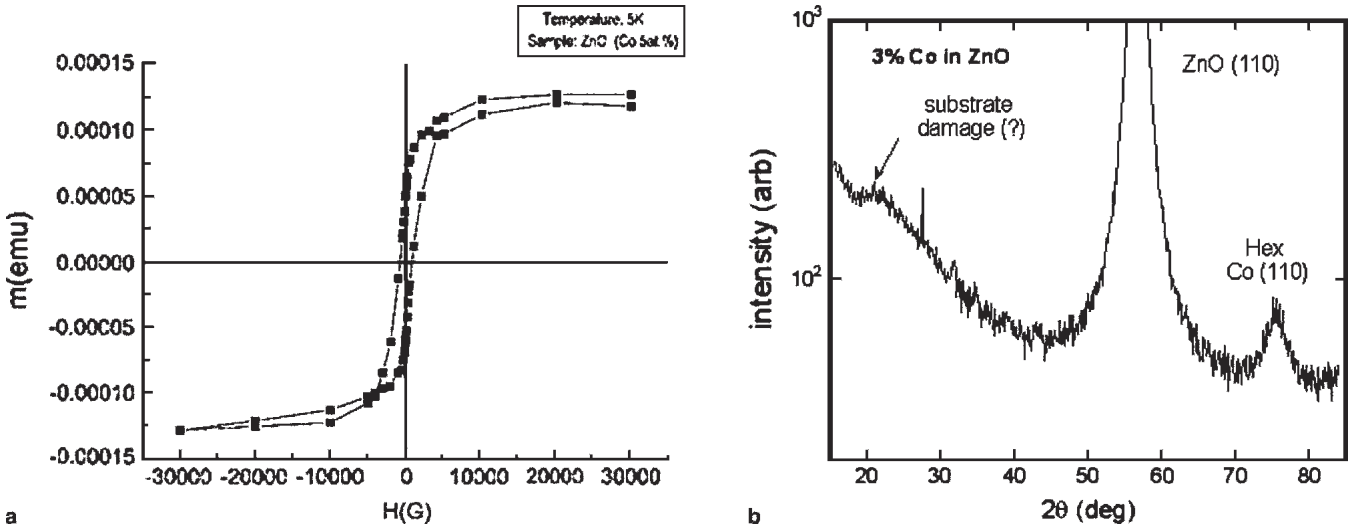

Fig. 2. Hysteresis loop in (a) Co-implanted ZnO and XRD spectra from the sample showing the (b) presence of oriented Co precipitates.

the use of wide bandgap semiconductors as sensitive gas and chemical sensors. ZnO is a piezoelectric, transparent wide bandgap semiconductor used in surface acoustic wave devices. Its bandgap can be increased by Mg-doping. ZnO has been effectively used as a gas sensor material based on the near-surface modification of charge distribution with certain surface-absorbed species. In addition, it is attractive for biosensors given that Zn and Mg are essential elements for neurotransmitter production and enzyme functioning. ZnO is attractive for forming various types of nanorods, nanowires, and nanotubes. The large surface area of the nanorods makes them attractive for gas and chemical sensing, and the ability to control their nucleation sites makes them candidates for high density sensor arrays. The sensing mechanism for chemical adsorbates in piezoelectric materials originates from compensation of the polarization-induced bound surface charge by interaction with the polar molecules in the liquids.

Single ZnO nanorods with ohmic contacts at either end exhibit large changes in current upon exposing the surface region to polar liquids introduced through an integrated microchannel. The polar nature of the electrolyte introduced leads to a change of surface charges on the nanorod, producing a change in surface potential at the semiconductor/liquid interface. The nanorods exhibit a linear change in conductance between pH 2–12 of 8.5 nS/pH in the dark and 20 nS/pH when illuminated with ultraviolet (UV, wavelength of 365 nm) light. The nanorods show stable operation with a resolution of ~0.1 pH over the entire pH range. The results indicate that ZnO nanorods may have application in integrated chemical, gas, and fluid monitoring sensors. The pH solution was made using a syringe autopipette (2–20 μL). A scanning electron micrograph (SEM) of the completed device is shown in Fig. 3.

Prior to the pH measurements, we used pH 4, 7, 10 buffer solutions from Fisher Scientific (Newark, NJ) to calibrate the electrode. The measurements at 25°C were carried out in the dark or under UV illumination from 365-nm light using an Agilent 4156C parameter analyzer to avoid parasitic effects. The pH solution was made by the titration method using HNO_3, NaOH, and distilled water. The electrode was a conventional Acumet standard Ag/AgCl electrode. The adsorption of polar molecules on the surface of ZnO affects the surface potential and device characteristics. Fig. 4 shows the conductance at a bias of 0.5 V as a function of time from nanorods exposed for 60 sec to a series of solutions whose pH was varied from 2 to 12. The current is significantly reduced upon exposure to these polar liquids as the pH is increased. The data in Fig. 4 show that the high-electron-mobility transistor (HEMT) sensor is sensitive to the concentration of the polar liquid and therefore could be used to differentiate between liquids into which a small amount of outflow of another substance has occurred.

Figure 5 shows the conductance of the nanorods in either the dark or during UV illumination at a bias of 0.5 V for different pH values. The nanorods exhibit a linear change in conductance between pH 2–12 of 8.5 nS/pH in the dark and 20 nS/pH when illuminated with UV (365 nm) light. The nanorods show stable operation with a resolution of ~0.1 pH over the entire pH range, showing the remarkable sensitivity of the HEMT to relatively small changes in concentration of the liquid.

There is still much to understand about the mechanism of the current reduction in relation to the adsorption of the polar liquid molecules on the ZnO surface. It is clear that these molecules are bonded by Van der Waal type interactions. They screen surface change that is induced by polarization in the ZnO. Different chemicals are likely to exhibit degrees of interaction with the ZnO surface.

ACKNOWLEDGEMENTS

The work at UF is partially supported by the AFOSR under Grant No. F49620-03-1-0370 (T. Steiner); NSF (CTS-0301178, monitored by

Table III. Summary of Reported Magnetism Results in ZnO

Compound	TM Content	Substrate	Fabrication Method	Growth Temperature (°C)	Oxygen Pressure (Torr)	Post annealing	T_c (K)	Notes
ZnO:Mn	<0.35	c-Sapphire	PLD	600	5×10^{-5}	—	N/A	—
ZnO:Mn	0.36	c-Sapphire	PLD	600	5×10^{-5}	—	N/A	Spin-glass
$Zn_{1-x}TM_xO$		c-Sapphire	PLD	500–600	1×10^{-9} to 10^{-6}	—	N/A	—
ZnO:Co	0.02–0.5	c-Sapphire	PLD	300–700	1×10^{-6} to 10^{-1}	—	—	Spin-glass
ZnO:Mn	0.01–0.36	c-Sapphire	PLD	610	5×10^{-5}	—	—	Paramagnetic
ZnO:(Co, Mn, Cr, or Ni)	0.05–0.25	r-Sapphire	PLD	350–600	$2–4 \times 10^{-5}$	—	280–300	2 μ_B/Co
ZnO:Ni	0.01–0.25	c-Sapphire	PLD	300–700	1×10^{-5}	—	—	Superpara- or ferromagnetic
ZnO:V	0.05–0.15	r-Sapphire	PLD	300	10^{-5} to 10^{-3}	—	>350	0.5 μ_B/V
ZnO:(Co, Fe)	<0.15	SiO_2/Si	Magnetron sputtering	600	2×10^{-3}	600°C, 10 min, 1.0×10^{-5} Ton	>300	12–15 emu/cm^3
ZnO:Co	0.03–0.05	Bulk ZnO	Ion implantation	—	—	700°C, 5 min under O_2	>300	Oriented Co precipitates
ZnO:Mn	0–0.25	c-Sapphire	Sol-gel	<350	—	700°C, 1 min	>350	0.56 μ_B/Co
ZnO:Mn	0–0.3	c-Sapphire	PLD	—	—	—	>30–45	0.15–0.17 μB/Mn
ZnO:Mn	<0.04	—	Sintered pellets	500–700	Air, atmospheric pressure	—	>425	0.006 emu/gm, single phase
ZnO:Mn	0.02	Fused quartz	PLD	400	—	—	>425	0.05 emu/g, single phase
ZnO:(Fe, Cu)	0–0.1	Solid-state reaction	897	—	—	—	550	0.75 μ_B/Fe
ZnO:Co	0.015		PLD	650	5×10^{-5}	—	>300	ferromagnetic
ZnO:(Co, A1)	0.04–0.12	Glass	RF sputtering	—	1×10^{-2} in Ar	—	>350	0.21 μ_B/Co
ZnO:Mn	0.04–0.09	c-sapphire	Reactive sputtering	200–380	—	—	>400	3μ_B/Co
ZnO:(Mn, Sn)	0–0.3	—	Implantation	—	—	5 min, 700°C	250	ferromagnetic

Fig. 3. Scanning electron microscopy of ZnO nanorod with integrated microchannel (4-μm width).

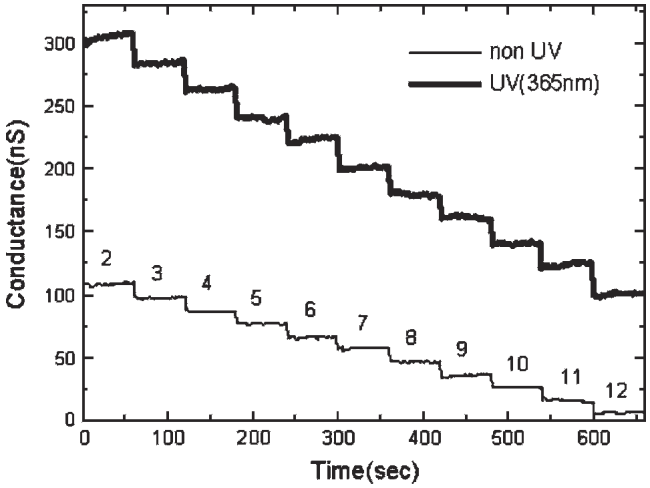

Fig. 4. Change in conductance with pH (from 2 to 12) at V = 0.5 V.

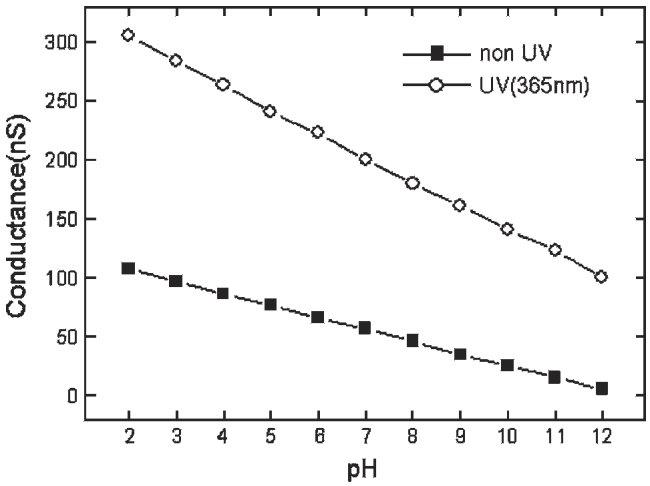

Fig. 5. Relation between pH and conductance of ZnO nanorod either with or without UV (365 nm) illumination.

Drs. M. Burka and D. Senich); NASA Kennedy Space Center Grant NAG 10-316, monitored by Mr. Daniel E. Fitch; ONR (Grant No. N00014-98-1-02-04, H.B. Dietrich); and NSF (DMR 0400416).

REFERENCES

1. S. von Molnar and D. Read, *Proc. IEEE* 91, 715 (2003).
2. H. Ohno, *J. Vac. Sci. Technol. B* 18, 2039 (2000).
3. T. Dietl, *Semicond. Sci. Technol.* 17, 377 (2002).
4. S.J. Pearton et al., *J. Appl. Phys.* 93, 1 (2003).
5. S.J. Pearton, C.R. Abernathy, D.P. Norton, A.F. Hebard, Y.D. Park, L.A. Boatner, and J.D. Budai, *Mater. Sci. Eng.* R40, 137 (2003).
6. T. Dietl, H. Ohno, F. Matsukura, J. Cibert, and D. Ferrand, *Science* 287, 1019 (2000).
7. K. Sato and H. Katayama-Yoshida, *Semicond. Sci. Technol.* 17, 367 (2002).
8. W. Prellier, A. Fouchet, B. Mercey, and J. Phys, *Condensed Matter* 15, R1583 (2003).
9. T. Fukumura, Y. Yamada, H. Toyosaki, T. Hasegawa, H. Koinuma, and M. Kawasaki, *Appl. Surf. Sci.* 131, 453 (2004).
10. Y. Matsumoto, M. Murakami, T. Shono, T. Hasegawa, T. Fukumura, M. Kawasaki, P. Ahmet, T. Chikyow, S. Koshihara, and H. Koinuma, *Science* 291, 854 (2001).
11. Y. Matsumoto, R. Takahashi, M. Murakami, T. Koida, X.J. Fan, T. Hasegawa, T. Fukumura, M. Kawasaki, S.Y. Koshihara, and H. Koinuma, *Jpn. J. Appl. Phys.* 40, L1204 (2001).
12. K. Sato and H. Katayama-Yoshida, *Jpn. J. Appl. Phys.* 39, L555 (2000).
13. K. Ueda, H. Tabata, and T. Kawai, *Appl. Phys. Lett.* 79, 988 (2001).
14. S.G. Yang, A.B. Pakhomov, S.T. Hung, and C.Y. Wong, *IEEE Trans. Magn.* 38, 2877 (2002).
15. N. Wakano, Y. Fujimura, N. Morinaga, A. Abe, N. Ashida, and T. Ito, *Physica E* 10, 260 (2001).
16. T. Fukumura, Z.W. Jin, A. Ohtomo, H. Koinuma, and M. Kawasaki, *Appl. Phys. Lett.* 75, 3366 (1999).
17. M. Berciu and R.N. Bhatt, *Phys. Rev. Lett.* 87, 108203 (2001).
18. T. Wakano, N. Fujimura, Y. Morinaga, N. Abe, A. Ashida, and T. Ito, *Physica C* 10, 260 (2001).
19. T. Fukumura, Z. Jin, A. Ohtomo, H. Koinuma, and M. Kawasaki, *Appl. Phys. Lett.* 75, 3366 (1999).
20. S.W. Jung, S.-J. An, G.-C. Yi, C.U. Jung, S.-I. Lee, and S. Cho, *Appl. Phys. Lett.* 80, 4561 (2002).
21. D.P. Norton, S.J. Pearton, A.F. Hebard, N. Theodoropoulou, L.A. Boatner, and R.G. Wilson, *Appl. Phys. Lett.* 82, 239 (2003).
22. D.P. Norton et al., *Appl. Phys. Lett.* 83, 2294 (2003).
23. K. Sato and H. Katayama-Yoshida, *Mater. Res. Soc. Symp. Proc. 666,* F4.6.1 (2001).
24. S.R. Shinde et al., *Phys. Rev. B: Condens. Matter Mater. Phys.* 67, 115211 (2003).
25. A. Punnoose, M.S. Seedra, W.K. Park, and J.S. Moodera, *J. Appl. Phys.* 93, 7867 (2003).
26. H. Nakagawa and H. Katayama-Yoshida, *Jpn. J. Appl. Phys.* 40, L1355 (2001).
27. M. Berciu and R.N. Bhatt, *Physica B* 312/313, 815 (2002).
28. A.C. Durst, R.N. Bhatt, and P.A. Wolff, *Phys. Rev. B: Condens. Matter Mater. Phys.* 65, 235205 (2002).
29. J.-H. Kim, H. Kim, D. Kim, Y.-E. Ihm, and W.-K. Choo, *J. Appl. Phys.* 92, 6066 (2002).
30. H. Saeki, H. Tabata, and T. Kawai, *Solid State Commun.* 120, 439 (2001).
31. Y.M. Cho, W.-K. Choo, H. Kim, D. Kim, and Y.-E. Ihm, *Appl. Phys. Lett.* 80, 3358 (2002).
32. H.J. Lee, S.Y. Jeong, C.R. Cho, and C.H. Park, *Appl. Phys. Lett.* 81, 4020 (2002).
33. P. Sharma, A. Gupta, K.V. Rao, F.J. Owens, R. Sharma, R. Ahuja, J.M. Osorio Guillen, B. Johansson, and G.A. Gehring, *Nature Mater.* 2, 673 (2003).
34. S.J. Hahn, J.W. Song, C.H. Yang, S.H. Park, J.H. Park, Y.H. Jeong, and K.W. Rhie, *Appl. Phys. Lett.* 81, 4212 (2002).
35. K. Rode, A. Anane, R. Mattana, J.-P. Contour, O. Durand, and R. LeBourgeois, *J. Appl. Phys.* 93, 7676 (2003).
36. N. Theordoropoulou et al. (to be published).